Title

A nut-and-bolt assembly of the bimodular large progenitor botulinum neurotoxin complex

Journal

Science Advances, 11(35)

ISSN

2375-2548

Authors

Lam, Kwok-Ho
Gao, Linfeng
Przykopanski, Adina
et al.

Publication Date

2025-08-29

DOI

10.1126/sciadv.adx5831

STRUCTURAL BIOLOGY

A nut-and-bolt assembly of the bimodular large progenitor botulinum neurotoxin complex

Kwok-ho Lam[1]†, Linfeng Gao[1]†, Adina Przykopanski[2], Baohua Chen[1], Ting Huang[1], Maren Krüger[3], Anna-Magdalena Bartels[2], Martin Bernhard Dorner[3], Kay Perry[4], Brigitte Gertrud Dorner[3], Andreas Rummel[2]*, Rongsheng Jin[1]*

Botulinum neurotoxin serotype A (BoNT/A) is naturally produced by bacteria along with four nontoxic neurotoxin-associated proteins (NTNH, HA70, HA33, and HA17), forming a bimodular large progenitor toxin complex (L-PTC). The BoNT/A–NTNH complex protects the toxin from adverse environment, while the complex consisting of HA proteins facilitates toxin absorption during oral intoxication. How these two independent modules assemble into the L-PTC remains unclear. Here, we report the crystal structure of the BoNT/A–NTNH–HA70 complex at ~2.9-Å resolution. The structure reveals that the BoNT/A–NTNH complex is anchored into a concentric double β-barrel channel of trimeric HA70 through a short β-hairpin of NTNH (termed nLoop), resembling a nut-and-bolt attachment. We find that the nLoop of NTNH is strictly conserved across HA-containing BoNT complexes and that NTNH–HA70 binding is interchangeable among them. Furthermore, we demonstrate that the nLoop functions as a minimal motif enabling attachment of a protein-of-interest to the HA complex, with potential applications in oral biologics delivery.

INTRODUCTION

Botulinum neurotoxins (BoNTs) are the most lethal toxins in nature, which are produced predominantly by *Clostridium botulinum* and a few related species (*1*). They are distinguished into seven major serotypes (A to G) which can be further separated into a number of subtypes (*2*). All BoNTs are encoded in either the hemagglutinin *ha* toxin gene cluster or the *orfX* toxin gene cluster in BoNT-producing bacteria (*3*). Both toxin gene clusters carry the BoNT-encoding gene and a gene encoding a protein termed nontoxic nonhemagglutinin (NTNH). In addition, the *ha* cluster encodes three hemagglutinin proteins (HA17, HA33, and HA70), while the *orfX* cluster encodes OrfX1, OrfX2, OrfX3, and P47. These non-BoNT proteins are collectively termed neurotoxin-associated proteins, which, together with BoNT, assemble into progenitor toxin complexes (PTCs) of varying sizes and compositions.

Each BoNT is composed of a ~50-kDa light chain (LC) and a ~100-kDa heavy chain (HC), and the HC is composed of an N-terminal translocation domain (H_N) and a C-terminal receptor binding domain (H_C). NTNH has evolved as a pseudo-enzyme of BoNT, sharing a similar structure but lacking its toxicity. Its three domains—nLC, nH_N, and nH_C—are named on the basis of their homology to the corresponding BoNT domains (Fig. 1A) (*4*–*6*). Intriguingly, NTNHs of the hemagglutinin (HA)-type BoNTs (e.g., BoNT/A1, A5, B1-B8, C, CD, D, DC, and G) have a unique insert in their nLC (Gly^{116}–Ala^{148} in NTNH of BoNT/A1, termed nLoop) that is absent in the LC of BoNT. Furthermore, the nLoop is missing in NTNHs of the OrfX-type BoNTs (e.g., BoNT/A1-A4, A6-A8, E1-12, F19, HA, X, and J) (*4*–*7*). Only BoNT/A1, drug substance of Botox, can be produced by different *C. botulinum* strains carrying either the *ha* or the *orfX* toxin gene clusters, and only the corresponding NTNH/A1 encoded in the *ha* gene cluster harbors an nLoop (*8*).

Irrespective of the *ha* or the *orfX* toxin gene cluster, all BoNTs assemble with their corresponding NTNH into a ~290-kDa minimal PTC (M-PTC) (*4*–*6*, *9*–*11*). The M-PTC adopts a compact structure that provides mutual protection for BoNT and NTNH, enabling their survival in harsh environments such as acidic pH and digestive proteases in the gastrointestinal (GI) tract (*4*–*6*). For the HA-type BoNTs, the M-PTC can further associate with HA17, HA33, and HA70 to form a large PTC (L-PTC), reaching sizes of up to ~760 kDa (*5*, *7*, *12*). The oral toxicity of BoNTs is markedly increased in the form of the L-PTC (*13*, *14*). This is accomplished by two complementary processes: NTNH directly interacts with BoNT and protects it in the hostile GI environment, while the HA complex facilitates toxin absorption across the intestinal barrier via cell surface carbohydrates and the host epithelial cell adhesion protein E-cadherin (*4*, *7*, *15*–*26*). The OrfX proteins and P47 also enhance the oral toxicity of OrfX-containing BoNTs after in situ proteolytic activation by digestive proteases, although the underlying mechanisms remain elusive (*8*, *27*).

Only low-resolution electron microscopy structures are available for L-PTC/A and L-PTC/B, revealing an Apollo lunar module-like architecture, where the M-PTC resembles the "ascent stage" and the HA proteins form a three-arm heterododecameric complex representing the "descent stage" (*7*, *12*). It is speculated that the association of the M-PTC and the HA complex could be mediated by the nLoop of NTNH and HA70 (*4*, *28*–*33*). However, the structure and function of the nLoop remain elusive. Meanwhile, HA70, composed of three domains (D1 to D3), forms a homotrimer with many intriguing yet puzzling features (*5*, *7*, *21*). For instance, the D3 of HA70 can recognize carbohydrates and provide the framework to engage HA17 and HA33, with HA33 also capable of binding carbohydrates (*7*, *34*, *35*). The D3 and D2 of HA70, together with HA17, interact with E-cadherin to disrupt the intestinal epithelial barrier.

[1]Department of Physiology and Biophysics, University of California, Irvine, CA 92697, USA. [2]Institute for Toxicology, Hannover Medical School, Carl-Neuberg-Strasse 1, 30625 Hannover, Germany. [3]Biological Toxins, Centre for Biological Threats and Special Pathogens, Robert Koch Institute, Seestrasse 10, 13353 Berlin, Germany. [4]NE-CAT and Department of Chemistry and Chemical Biology, Cornell University, Argonne National Laboratory, Argonne, IL 60439, USA.
*Corresponding author. Email: r.jin@uci.edu (R.J.); rummel.andreas@mh-hannover.de (A.R.)
†These authors contributed equally to this work.

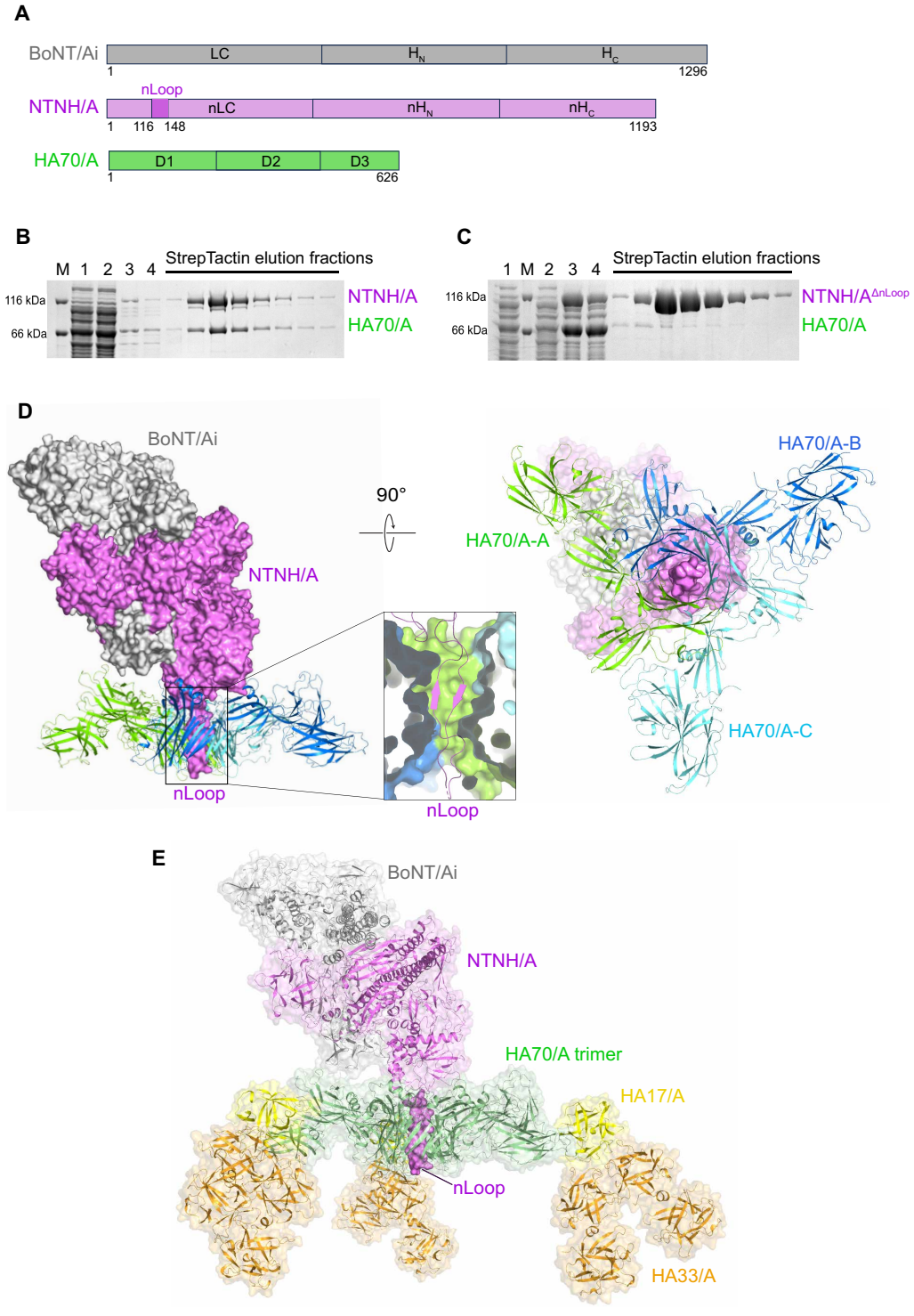

Fig. 1. Overall structure of M-PTC/A in complex with HA70/A trimer. (**A**) Schematic diagrams showing the domain organization of BoNT/Ai, NTNH/A, and HA70/A. (**B** and **C**) Deleting the nLoop of NTNH/A disrupts its association with HA70/A. NTNH/A with an N-terminal His-tag and C-terminal Strep-tag (B) or an nLoop-deleted variant (NTNH/A$^{\Delta nLoop}$) (C) was coexpressed with His-tagged HA70/A. These proteins were first isolated by immobilized metal affinity chromatography (IMAC) and subsequently by Strep-Tactin matrix. The representative Strep-Tactin elution fractions were analyzed by SDS-polyacrylamide gel electrophoresis (SDS-PAGE) and Coomassie staining. Lane M, marker; lane 1, cleared cell lysate; lane 2, IMAC flow-through; lane 3, IMAC eluate; lane 4, Strep-Tactin flow-through. (**D**) Cartoon and surface representations of the M-PTC–HA70 complex in two different views. BoNT/Ai and NTNH/A are shown as light gray and violet surfaces, respectively. The three HA70 protomers are colored green, cyan, and blue, respectively. (**E**) Cartoon and surface representations of the modeled L-PTC/A, assembled based on the structures of the M-PTC–HA70 complex and the HA70^{D3}–HA17–HA33 complex (PDB: 4LO7) (BoNT/Ai, light gray; NTNH/A, violet; HA70 trimer, pale green; HA17, yellow; HA33, orange).

The D1 and D2 domains of HA70 are organized as a pseudo–pore-forming toxin, forming a double-layered β-barrel at the center of trimeric HA70. This structure is homologous to the prepore conformation of *Clostridium perfringens* enterotoxin (CPE) and aerolysin from *Aeromonas hydrophila* despite HA70 being generally considered nontoxic (*36*–*38*).

Here, we report the crystal structure of a BoNT–NTNH–HA70 complex of BoNT/A1 in a 1:1:3 stoichiometry at ~2.9-Å resolution. The structure reveals that NTNH and HA70, as two pseudotoxins, mediate the assembly of the bimodular L-PTC. The nLoop of NTNH forms a β-hairpin that inserts into a concentric double β-barrel channel of the trimeric HA70, reminiscent of a nut-and-bolt connection. We find that the nLoop is highly conserved across HA-type BoNT complexes, and the binding between NTNH and HA70 is interchangeable among them, indicating a conserved mode of L-PTC assembly. Furthermore, we demonstrate that the nLoop can be used as a versatile targeting module to attach proteins of interest (POIs) to the HA complex via HA70, suggesting that we could potentially repurpose BoNT's delivery vehicle for drug delivery applications.

RESULTS

Structures of the BoNT–NTNH–HA70 complex and the fully assembled L-PTC

The NTNHs encoded in *ha* toxin gene cluster have a unique nLoop that is missing in those encoded in *orfX* toxin gene clusters (*4*–*7*); however, its structure and function remain elusive. We found that the nLoop is indispensable for the assembly of the M-PTC with the HA complex to form the L-PTC, as its deletion from NTNH coexpressed with BoNT/A1 (referred to as NTNH/A) abolished its ability to associate with HA70/A (Fig. 1, B and C). It thus raises an intriguing question about how the small nLoop is capable of bridging two large molecular weight complexes—the ~290-kDa M-PTC and the ~470-kDa HA complex.

To determine the structure of the fully assembled L-PTC/A, we made extensive efforts to crystallize the reconstituted L-PTC/A using an inactive form of BoNT/A (E224Q/R363A/Y366F, BoNT/Ai) along with recombinant NTNH/A and the HA complex (*4*). However, we were unable to obtain diffractible crystals, likely due to the flexibility of the HA17–HA33 arms, which may hinder crystal packing (*7*). Consequently, we shifted our focus to studying the more stable M-PTC–HA70 complex, which is the core of the L-PTC. To facilitate crystal packing and improve the diffraction of crystals, we screened a large panel of BoNT/A-binding VHHs, the antigen-binding region (V_H) of the heavy-chain-only antibodies (also known as nanobodies or single-domain antibodies), taking advantage of numerous BoNT/A-binding VHHs we have been developing as reagents and countermeasures (*4*, *39*–*43*). We also combined these VHHs with the Fab fragments of a few NTNH/A-binding monoclonal antibodies to further facilitate crystal packing (the development and characterization of these antibodies will be published in an independent paper).

After extensive crystallization screening and optimization, we determined the crystal structure of the M-PTC–HA70 complex at 2.9-Å resolution, facilitated by BoNT/A-binding VHH-F12, VHH-H7, and an NTNH/A-binding Fab (table S1). There is one copy of the M-PTC–HA70–VHH-F12–VHH-H7–Fab supercomplex in each asymmetric unit (fig. S1). The overall structure of the complex reveals that the M-PTC sits atop the trimeric HA70/A complex, which is similar to observations from prior low-resolution electron microscopy (EM) studies (Fig. 1, D and E) (*7*, *12*). The two VHHs bind to the LC of BoNT/A, which is consistent with our prior studies (*40*, *43*), while the Fab binds to the nH_N of NTNH/A. As these VHHs and the Fab do not affect the interaction between the M-PTC and HA70, they are not discussed further in this paper for clarity.

The overall structures of the standalone M-PTC/A (PDB: 3V0A) and the HA70-bound form are almost identical, with a root mean square deviation (RMSD) of 0.93 Å over 2411 superimposable residues, except for a slight tilt of nLC in the M-PTC–HA70 complex (fig. S2A). The M-PTC-bound HA70 forms a trimer with a structure highly similar to that of the standalone HA70 trimer [Protein Data Bank (PDB): 4LO4] (*7*). Pair-wise superposition across three HA70 molecules yields RMSD of 1.1 Å (582 residues), 1.49 Å (585 residues), and 0.99 Å (590 residues), respectively, indicating no large structural change upon complex formation (fig. S2B). In both cases, the trimeric HA70 creates a central cylindrical β-barrel, which measures ~33 Å in length and ~21 Å in diameter. To facilitate discussion, we refer the three HA70/A protomers as HA70/A-A, HA70/A-B, and HA70/A-C thereafter.

Nevertheless, the structure of the M-PTC–HA70 complex reveals remarkable insights into the assembly of the L-PTC. For instance, the nLoop of NTNH/A (Gly^{116}–Ala^{148}), which is invisible in the structure of standalone M-PTC, adopts a β-hairpin conformation in the M-PTC-HA70 complex (Fig. 1D). Moreover, it inserts and penetrates through the central pore-like channel of HA70 trimer, resembling a nut-and-bolt connection (Fig. 1, D and E) (*4*–*7*). These findings reveal the long sought-after missing link between the M-PTC and the HA complex, two structurally and functionally distinct modules of the L-PTC (*7*). On the basis of the crystal structure of the M-PTC–HA70 complex, the central component of the L-PTC, we constructed a fully assembled L-PTC/A by aligning the crystal structure of the mini-HA complex ($HA70^{D3}$–HA17–HA33, PDB: 4LO7) with each $HA70^{D3}$ (Fig. 1E). This high-resolution model of the L-PTC, consisting of 14 subunits with a total mass of ~760 kDa, aligns well with our previous low-resolution EM density map while now providing complete atomic details (fig. S3) (*7*).

Extensive contacts between NTNH/A and HA70/A

The interactions between NTNH/A and HA70/A buried a large interface area of ~2000 $Å^2$ per molecule (PDBePISA), which is comparable to the size of the interface between NTNH/A and BoNT/A (*4*). Most of the interactions are mediated by the nLoop of NTNH/A that inserts into the central pore of HA70 trimer. Despite the pseudo-symmetric nature of the HA70/A trimer, NTNH/A interacts with the three HA70/A molecules in an asymmetrical manner. For example, the insertion of nLoop induces specific conformational changes in several surface loops of one HA70 unit (HA70/A-C) surrounding the HA70 pore, including loop-250, loop-285, and loop-65. Loop-250 moves away from the center of the pore, while loop-285 changes from a loop to a helix (fig. S2, C and D). These loops are involved in direct contacts with NTNH nLoop, and their conformational changes are necessary to accommodate the M-PTC that would otherwise sterically clash with the nLoop (fig. S2E).

Besides extensive interactions involving the nLoop of NTNH/A and the central pore of HA70 trimer that will be discussed in more details in the next section, NTNH/A and BoNT/A establish two interfaces with the "upper" surface of HA70 trimer. For example, NTNH/A engages with two HA70/A molecules, HA70/A-A and

HA70/A-B, through its loop-310 and loop-470, respectively (Fig. 2, A and C and D). More specifically, NTNH/A-D315 and NTNH/A-D470 electrostatically interact with Q100/R253 and R253/N254 of HA70/A-B, respectively, while the backbone atoms of NTNH/A-N314 and NTNH/A-I312 interact with N66 of the same HA70/A-B (Fig. 2, C and D). In addition, NTNH/A-N310 and NTNH/A-G308 form H-bonds with R251 and R253 of HA70/A-A, respectively (Fig. 2C). We also found a small interface (~189 Å^2) between the H_C of BoNT/A and HA70/A-A: BoNT/A-K1187 forms an H-bond with N381 of HA70/A-A, while BoNT/A-Y1191 and BoNT/A-K1189 have hydrophobic interactions with I400 of HA70/A-A (Fig. 2B). This is consistent with the prior EM structure of the L-PTC (*7*), suggesting that BoNT/A plays only a minimum role in the M-PTC–HA70 interaction. Therefore, BoNT/A can be readily released from the L-PTC at neutral pH upon absorption from the GI tract (*4*). The extensive contacts between the "upper" surface of the HA70 trimer and the M-PTC ensure that the nLoop only inserts into the HA70 central pore from one side.

Multilayered interactions between the nLoop of NTNH/A and HA70/A

The extensive interactions between the nLoop of NTNH/A and HA70/A can be divided into three layers across the central HA70 pore (Fig. 3A). The most NTNH/A proximal layer of the HA70 pore primarily involves hydrophobic interactions with NTNH: NTNH/A-M122 binds L63, I248, and P250 of HA70/A-A; NTNH/A-Y147 binds V65, P102, L252, and R253 of HA70/A-B; NTNH/A-I143 and F125 interact with L63, I248, P250, L252, and L292 of HA70/A-B and I59, L63, and I248 of HA70/A-C; NTNH/A-F145 and NTNH/A-I123 interact with a hydrophobic pocket lined with L63, V65, P102, I248, P250, L252, and L292 of HA70/A-C (Fig. 3, B and C). Notably, several identical amino acids of the three HA70 units are involved in nLoop binding.

The middle layer of the HA70 pore is featured with a cluster of six oppositely charged residues, E106 and K294 from each HA70, which interact with a constriction region of the nLoop. These include interactions between T124 of NTNH/A and E106 of HA70/A-A, S140 of NTNH/A and K294 of HA70/A-A, F125 of NTNH/A and S141/K294 of HA70/A-B, and G126 of NTNH/A and S127/E106 of HA70/A-C (Fig. 3D).

At the bottom layer of the HA70/A pore, L138 of NTNH/A, located in a short 3_{10} helix of the nLoop, is buried in a pocket formed by I59, E106, S108, S244, G245, S246, and V296 of HA70/A-A. These interactions are further strengthened by hydrophobic interactions between NTNH/A-I139 and T57/I59 of HA70/A-B, as well as V296 of HA70/A-A, in addition to a hydrogen bond between NTNH/A-S137 and S108 of HA70/A-A, and a salt bridge between NTNH/A-K130 and E298 of HA70/A-C (Fig. 3E). The nLoop of NTNH/A penetrates the whole HA70 pore, and its distal tip emerges from the opposite side of the HA70 pore. Residues S131 and N132, located at

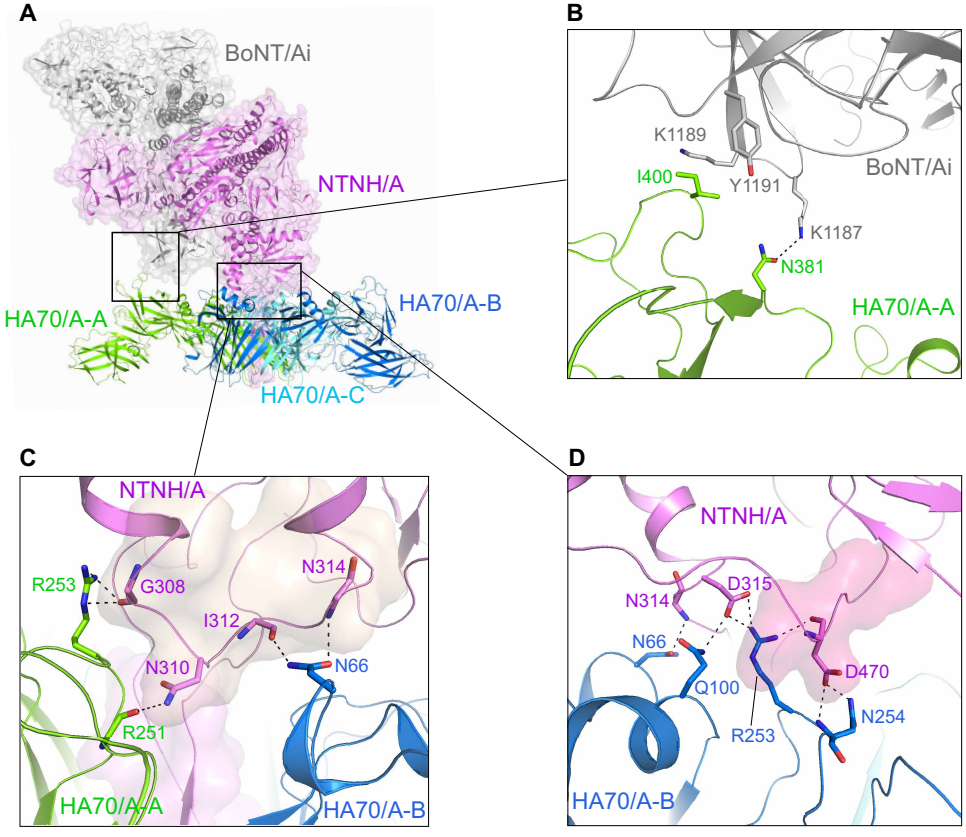

Fig. 2. Interactions between the M-PTC and HA70 outside the nLoop. (**A**) M-PTC interacts with HA70 via a major interface mediated by the nLC of NTNH and a minor interface involving the H_C of BoNT/Ai. (**B**) Close-up view of the interactions between BoNT/Ai (light gray) and one HA70 protomer (unit A, green). (**C** and **D**) Close-up views of the interactions between loop-310 and loop-470 of NTNH/A and two HA70 protomers (unit A in green and unit B in blue). Key interacting residues are shown in sticks.

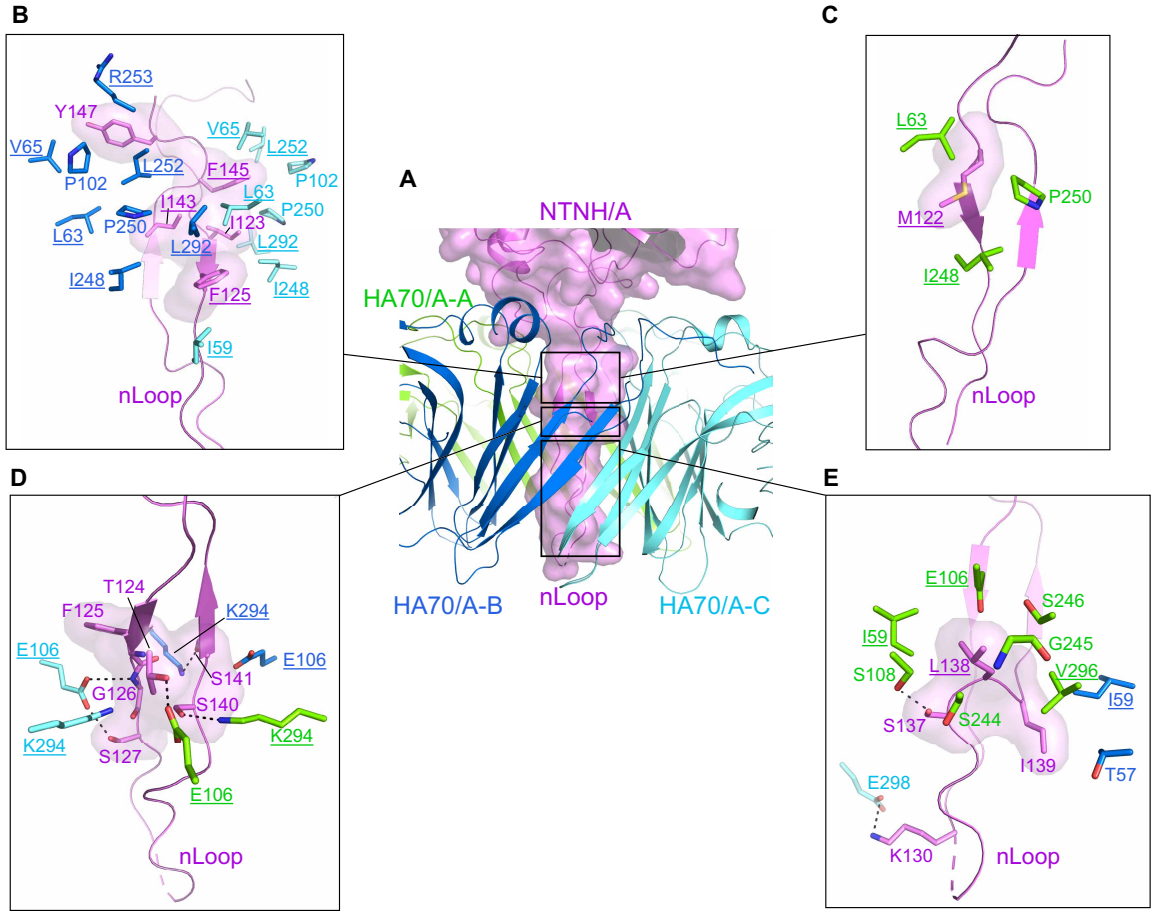

Fig. 3. Multilayered interactions between NTNH nLoop and HA70. (**A**) The nLoop of NTNH/A inserts into HA70/A pore through multilayered interactions in a nut-and-bolt fashion. (**B** to **E**) Close-up views of nLoop–HA70 interface at the proximal [(B) and (C)], middle (D), and bottom layers (E). NTNH/A is colored violet, and HA70/A-A, HA70/A-B, and HA70/A-C are colored green, cyan, and blue, respectively. Key interacting residues are shown as sticks.

the tip of the nLoop, have no visible electron density, likely being flexible and not interacting with HA70.

It is worth noting that the trimeric HA70 is organized as an aerolysin-like pseudo–pore-forming toxin, forming two concentric β-barrels at the center despite HA70 being nontoxic (Fig. 4, A and B) (*36*–*38*). More specifically, 12 β-strands—two from D1 and two from D2 of each HA70—form the inner β-barrel of the pore, while 18 β-strands—three from D1 and three from D2 of each HA70—make up the outer β-barrel (Fig. 4, C to E). The nLoop of NTNH inserts into the HA70 pore from one side, with its distal tip emerging from the opposite side, resembling a nut-and-bolt connection. All interactions are established between the nLoop of NTNH/A and the inner pore of HA70, while the outer pore of HA70 likely serves to stabilize the inner pore.

The nLoop plays a dominant role in mediating the interactions between NTNH and HA70

To better understand the interactions between the HA70 pore and the nLoop of NTNH, we designed a series of mutants of HA70/A and NTNH/A that carry mutations on key interacting residues and then examined how these mutations affected NTNH–HA70 association (Fig. 5A). Because NTNH and HA70 only form a complex when they are coexpressed (*7*, *21*), mutants of His-green fluorescent protein (GFP)-tagged NTNH/A and His-tagged HA70 were coexpressed pairwise in *Escherichia coli*. Both proteins were copurified by Ni–nitrilotriacetic acid (NTA) affinity resins, and the NTNH–HA70 complex was subsequently precipitated using the same anti-NTNH/A monoclonal antibody that was used to facilitate crystallization. On the basis of their intensities on the SDS-polyacrylamide gel electrophoresis (SDS-PAGE) gels (Source Data), the wild-type (WT) NTNH–HA70 complex showed a ~1:1.5 mass ratio of NTNH:HA70, which is consistent with 1:3 molar ratio of NTNH:HA70.

We found that mutating residues outside the nLoop of NTNH/A, such as those in loop-310 that loosely touches the surface of HA70 (e.g., G308N/A310Y), did not substantially affect their interaction (Fig. 5A). We then introduced mutations at various regions of the nLoop throughout the entire HA70 pore. We found that most single-point mutations on the nLoop of NTNH/A such as M122K, I143K, and F145K that bind to the upper layer of the HA70 pore, or F125K and P129K that interact with the middle and lower layers of the HA70 pore, respectively, had little to no effect on their interaction with HA70/A (Fig. 5A). This finding suggests that HA70 could tolerate limited amino acid variations in the nLoop of NTNH/A. Nevertheless, double mutations on the nLoop, such as F125K/I143K and F125K/F145K, led to more severe disruption of HA70 binding.

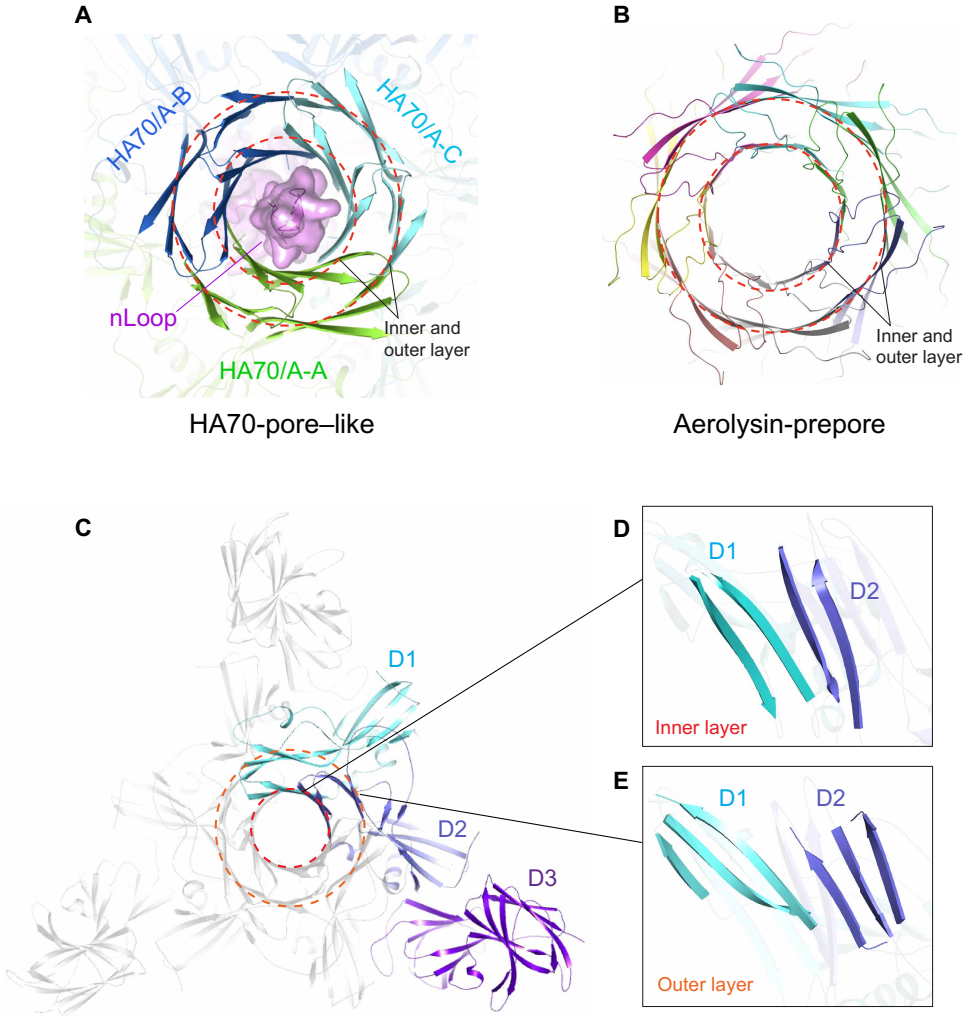

Fig. 4. Trimeric HA70 forms a two-layered β-barrels pore for nLoop insertion. (**A** and **B**) Structural comparison between HA70 concentric β-barrels in the M-PTC–HA70 complex (A) and aerolysin prepore (B). (**C** to **E**) In each of the three HA70 units forming a trimer, the D1 domain (cyan) and the D2 domain (slate) contribute two β-strands each to form the inner β-barrel and three β-strands each to form the outer β-barrel.

However, L138 of NTNH/A, which is located in a short 3_{10} helix and interacts with the bottom layer of the HA70 pore (Fig. 3E), is crucial for HA70 binding, as L138K mutation in NTNH/A completely abolished their association (Fig. 5A). Introducing a positive net charge at L138 of NTNH/A is unfavorable as it is surrounded by a hydrophobic pocket on HA70/A-A, and the side chain of a Lys may also introduce steric hindrance in this area. Consistently, mutating L138-interacting residues on HA70, such as I59K and V296K, also severely disrupted their binding. These data show that the bottom layer of the HA70/A β-barrel plays a key role in mediating NTNH/A interaction. Mutations in the distal tip of the nLoop that emerges from the opposite side of the HA70 pore, such as K133A/K134A, had a minor effect on HA70 binding, suggesting that this region plays a minimal role in HA70 association.

We also performed complementary mutagenesis studies on HA70. We found that mutations introduced at the middle to lower layers of the HA70 β-barrel had a more substantial impact on its interaction with NTNH/A compared to those located at the upper layer. For example, mutating certain aliphatic residues at the middle layer of the HA70/A pore, such as I59K, I248K, L292K, and V296K, severely disrupted its binding to NTNH/A. In contrast, similar mutations at residues around the upper layer of the HA70 pore—such as L63K, V65K, L252K, R253A—had only a mild effect on the binding (Fig. 5A and fig. S4, A and B).

A notable feature of the HA70 pore is a charged strip situated in the middle of the HA70 β-barrel, composed of three lysine (K294) and three glutamate (E106) residues, which are critical for binding NTNH/A. Replacing them with an Ala residue or a residue with opposite charge (e.g., E106A, E106K, K294A, K294E, and E106A/K294A) strongly prevented NTNH/A binding. A double mutation involving charge swapping between these two residues, such as E106K/K294E, resulted in a mild disruption of the NTNH–HA70 binding, suggesting that the net charge of the HA70 β-barrel in this region may be critical for NTNH/A binding (Fig. 5A).

As crucial controls, we selected three HA70 mutants (I59K, I248K, and K294E) that exhibited the strongest reduction in NTNH/A binding as representatives to examine the potential effects of these mutations on the structural integrity of HA70/A. These HA70

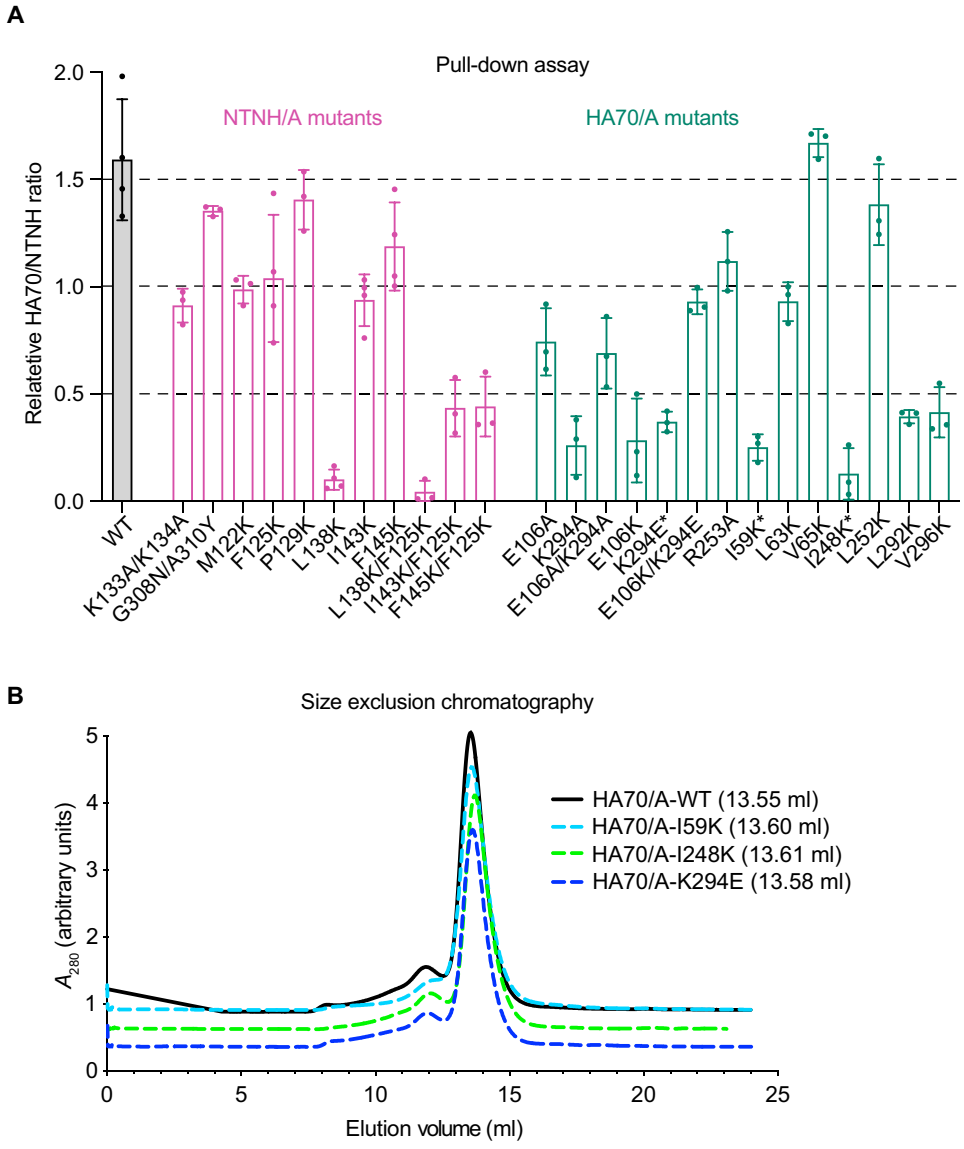

Fig. 5. Validation of the interactions between NTNH/A and HA70/A. (**A**) Pull-down assays examining the interactions between the NTNH/A mutants and the WT HA70/A or between the WT NTNH/A and HA70/A mutants. The coexpressed and copurified NTNH and HA70 were pulled down using immobilized anti-NTNH/A monoclonal antibody as bait and further analyzed by SDS-PAGE. Data are mean ± SD of relative HA70/NTNH ratio ($n = 3$). The signal of approximate 1:1.5 ratio of WT HA70 versus NTNH indicates a 1:3 molar ratio. (**B**) SEC analysis of WT HA70/A and selected mutants. The purity of the selected peak fractions was examined by SDS-PAGE and Coomassie staining (fig. S4). A_{280}, absorbance at 280 nm.

mutants showed identical migration patterns on size exclusion chromatography (SEC) compared to the WT HA70, indicating a WT-like folding and trimerization (Fig. 5B and fig. S4C). These findings demonstrate that these HA70 mutations specifically affect their ability to bind NTNH/A without compromising their overall structural integrity.

NTNH/A–HA70/A binding interface is highly conserved across HA-type BoNT complexes

The nLoop is a unique signature for NTNHs encoded in the *ha* toxin gene cluster and is absent in NTNHs encoded in the *orfX* toxin gene cluster, which do not have accompanying HA proteins (*4*–*7*, *44*–*46*). Twenty of the 33 residues in the nLoop (Gly^{116}–Ala^{148}) are strictly conserved in all known nLoop sequences of serotypes A, B, C, D, and G including the crucial L138 of NTNH/A. The nLoop sequences of NTNHs accompanying BoNT/A1, A5, and B1 to B8 are completely identical, highlighting the importance of this structural feature (fig. S5A). Sequence analyses of NTNH and HA70 indicate that the amino acid sequences at the binding interface are highly conserved across HA-type BoNTs (sequence identity of HA70, ~ 78%; NTNH, ~73%), suggesting that the binding mode between NTNH and HA70 is likely conserved across these BoNTs (fig. S5). We then asked whether NTNH and HA70 from different HA-containing BoNT serotypes could cross-interact with each other.

Accordingly, we cloned the genes encoding NTNH and HA70 of BoNT/A1, B1, D, and G (NTNH and HA70 of BoNT/C are nearly

identical to BoNT/D) and systematically coexpressed all pairs of NTNH and HA70 in *E. coli*. Initially, HA70 and NTNH were simultaneously purified from lysate by immobilized metal affinity chromatography (IMAC) via a His-tag on both proteins. Subsequently, we examined their interactions by a second affinity chromatography step using a Strep-tag exclusively fused to the C terminus of the NTNHs (Fig. 6). We found that NTNH/A coprecipitates HA70/A, B, and D in a ~1:1.5 mass ratio and HA70/G to a lesser amount, probably due to the lower expression rate of HA70/G. Similar results were observed for NTNH/B, D, and G, although the ratio of coprecipitated NTNH and HA70 varied, likely due to differences in their expression yields. These results thus demonstrate the exchangeability of nLoop-carrying NTNHs with HA70s from other serotypes. Hence, it is conceivable that chimeric L-PTCs could form as a result of recombination events between toxin gene clusters of different serotypes. For example, BoNT/C or D, which rarely causes human botulism partly due to its HA complex that does not bind human E-cadherin (*24*, *47*), could form a chimeric L-PTC with the HA complex of BoNT/A via NTNH/C or D, potentially altering species-specific oral toxicity and presenting challenges to public health.

The nLoop is a minimally required and transferable module for association with the HA complex

Our structural and mutagenesis results demonstrate that the nLoop plays a dominant role in mediating NTNH–HA70 association, and the binding mode is conserved across different BoNT serotypes. This led us to hypothesize that the nLoop might be transferable to an OrfX-type NTNH to establish novel associations with HA70. To this end, we genetically inserted the nLoop of NTNH/A into NTNH/E and NTNH/A2, respectively, which are both encoded in the *orfX* gene cluster and naturally lack the nLoop (Fig. 7A). The resulting constructs are termed NTNH/E^{nLoop} and NTNH/$A2^{nLoop}$. NTNH/E^{nLoop} carrying a glutathione *S*-transferase (GST)-tag and NTNH/$A2^{nLoop}$ carrying a His/Strep-tag were individually coexpressed with a His-tagged HA70/A in *E. coli*. NTNH/E^{nLoop} and HA70/A were first captured using Ni-NTA resins, followed by purification through Glutathione Sepharose 4B affinity chromatography. They could be coeluted from the glutathione resins following on-column cleavage of the GST-tag on NTNH, indicating successful complex formation (Fig. 7B). Consistent with this result, the NTNH/$A2^{nLoop}$–HA70/A complex could be pulled down via consecutive Co^{2+}-Talon and Strep-Tactin affinity purification (fig. S6). These results demonstrate that the nLoop inserted onto the OrfX-type NTNH is capable of attaching it to HA70. Moreover, we were able to assemble the NTNH/E^{nloop}–HA70/A complex with BoNT/Ei to form the M-PTC/E^{nLoop}–HA70/A complex, further validating the proper assembly of this novel chimeric complex mediated by the inserted nLoop (Fig. 7, C and D).

We then inspected the structure of the chimeric M-PTC/E^{nLoop}–HA70/A complex using negative-staining EM. Both the M-PTC/E^{nLoop} and the trimeric HA70/A could be clearly identified in the three-dimensional (3D) EM density map and 2D class averages, which allowed us to build a low-resolution structural model of the chimeric complex using the crystal structures of M-PTC/E (PDB: 4ZKT) and HA70/A (PDB: 4LO4) (Fig. 7, C and D) (*7*, *9*). The overall architecture of the M-PTC/E^{nLoop}–HA70/A complex highly resembles the crystal structure of the M-PTC/A–HA70/A complex, where the ovoid-shaped M-PTC/E with the engineered NTNH/E^{nLoop} lands on the top of the triangle-shaped HA70/A complex. We observed a ~45° rotation of the M-PTC/E^{nLoop} compared to the M-PTC/A when they associate with the trimeric HA70/A (fig. S7A). This is likely due to sequence variations in interacting areas outside the nLoop, including the HA70-interacting loop-310 and loop-470 on NTNH/E and the small HA70-interacting area on BoNT/E, which are not optimal for cross-serotype interactions with HA70/A.Consequently, the nLoop acts as the primary anchoring point, allowing M-PTC/E^{nLoop} to take a slightly different orientation relative to the HA complex (fig. S7B). Nevertheless, transplanting an nLoop to the

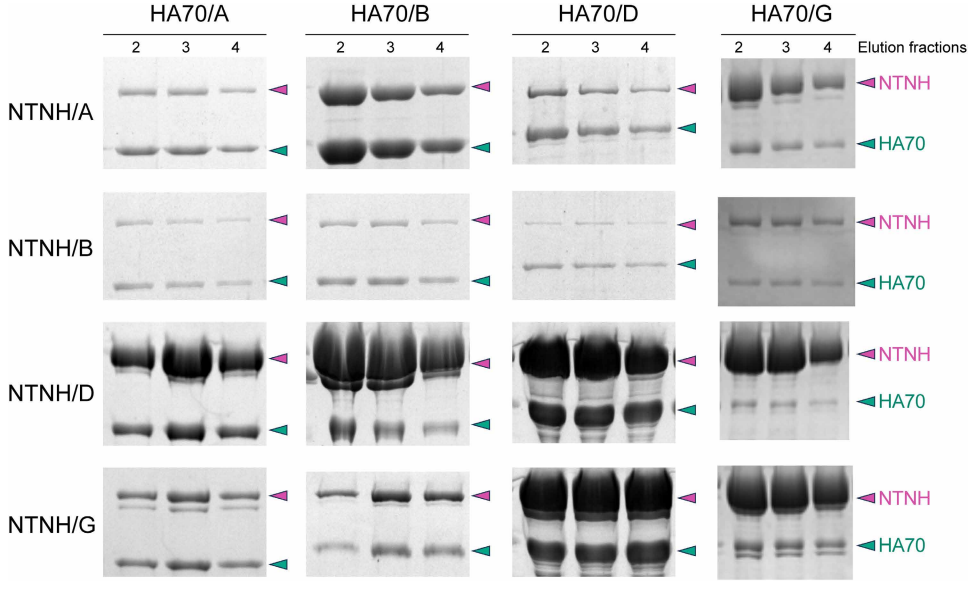

Fig. 6. Analysis of cross-serotype interactions between NTNH and HA70. Pairwise coexpressed His-tagged HA70 and His/Strep-tagged NTNH from serotypes A1, B1, D, and G were first captured using a Co^{2+}-Talon matrix, and the eluted fractions were further purified using Strep-Tactin resins. The Strep-Tactin elution fractions were analyzed by 10% SDS-PAGE, followed by Coomassie staining with fractions 2 to 4 shown as representatives.

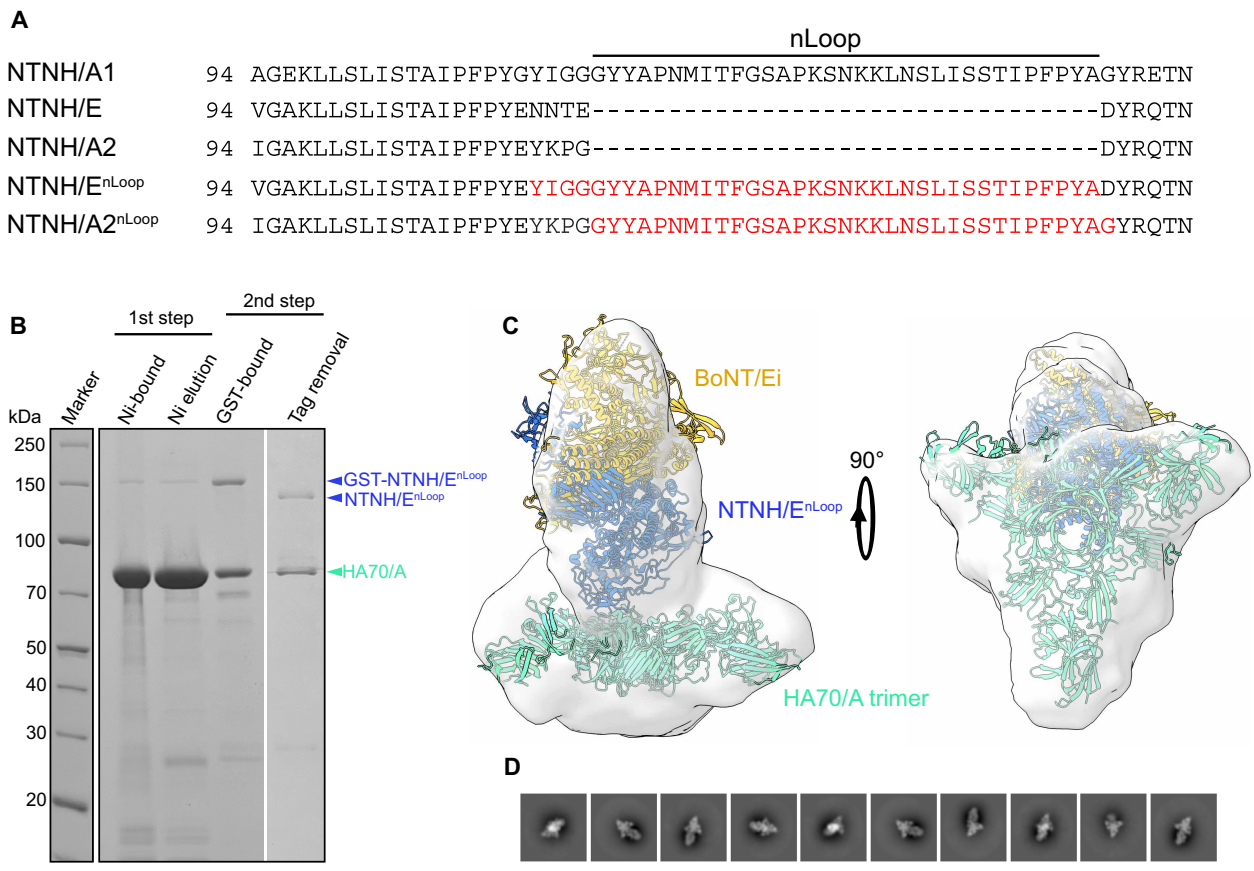

Fig. 7. An inserted nLoop in NTNH/E establishes novel association with HA70/A. (**A**) Amino acid sequence alignment among NTNH/A1, NTNH/E, NTNH/A2, and the engineered NTNH/E^{nLoop} and NTNH/A2^{nLoop} around the nLoop. (**B**) Copurification of the NTNH/E^{nLoop}–HA70/A complex. The coexpressed His-tagged HA70/A and GST-tagged NTNH/E^{nLoop} were first captured by Ni-NTA, and the eluted fraction was further purified by GST resin followed by on-column cleavage for GST removal. (**C**) Structural illustration of docking the crystal structures of M-PTC/E (PDB: 4ZKT) and HA70/A trimer (PDB: 4LO4) into an EM map generated from negative staining study of the M-PTC/E^{nLoop}–HA70/A complex (BoNT/Ei, yellow; NTNH/E, blue, HA70/A, green). (**D**) Representative 2D class averages of the M-PTC/E^{nLoop}–HA70/A complex.

OrfX-type NTNH/E or NTNH/A2 is sufficient to enable their attachment to HA70/A.

These compelling findings suggest that the nLoop could serve as a universal targeting module for tethering a protein of interest (POI) to the HA complex of BoNT via HA70. As a proof of concept, we designed two different fusion proteins, where an nLoop is inserted to a surface-exposed flexible loop in GFP between residues V171 and G174 (GFP^{nLoop}) or a loop in the middle of a leucine zipper followed by a C-terminal GFP (Zipper^{nLoop}-GFP), mimicking the way the nLoop is displayed by NTNH (Fig. 8, A and B). These two proteins carrying the nLoop were coexpressed with a His-tagged HA70/A in *E. coli*, and we then used two different methods to examine their potential interactions with HA70/A. GFP^{nLoop} forms a stable complex with HA70/A as evidenced by their comigration on SEC, while Zipper^{nLoop}-GFP and HA70/A can be coimmunoprecipitated by an anti-GFP VHH (Fig. 8, C to E). These results demonstrate that the nLoop functions as a minimally required HA70-binding motif. Furthermore, due to its small size, the nLoop can be inserted to a loop on a POI or attached to its N or C terminus via a small carrier protein, such as a leucine zipper. Hence, the nLoop would have minimal impact on the physiological activities of the POI while enabling its access to the delivery vehicle of BoNT.

DISCUSSION

The M-PTC and the HA complex are two structurally and functionally independent modules of BoNTs encoded in the *ha* toxin gene cluster, which are responsible for protecting and delivering BoNTs during oral intoxication. Here, we reveal the long sought-after missing link between them, allowing us to construct the first high-resolution atomic model of a fully assembled 14-subunit L-PTC/A (Fig. 1E). The nLoop of NTNH/A, which is missing in NTNHs encoded in the *orfX* toxin gene clusters, forms a β-hairpin that inserts into a concentric double β-barrel channel of a trimeric HA70/A, reminiscent of a nut-and-bolt attachment. Structure-based mutagenesis studies show that the nLoop plays a dominant role in mediating NTNH–HA70 association. Furthermore, this nLoop is highly conserved across NTNHs encoded in the *ha* toxin gene cluster, and the interaction between NTNH and HA70 is interchangeable among them, indicating a conserved mode of toxin complex assembly.

The trimeric HA70 pore is structurally similar to the prepore of aerolysin, with both featuring a concentric double β-barrel channel despite their low amino acid sequence similarity (fig. S8, A and B) (*36*, *48*). Aerolysin-like β-pore-forming toxins have divergent structures and sequences, but they have a common mode of action in that they have a stretch of amphipathic residues, which can transform into a β-hairpin that subsequently oligomerize into a

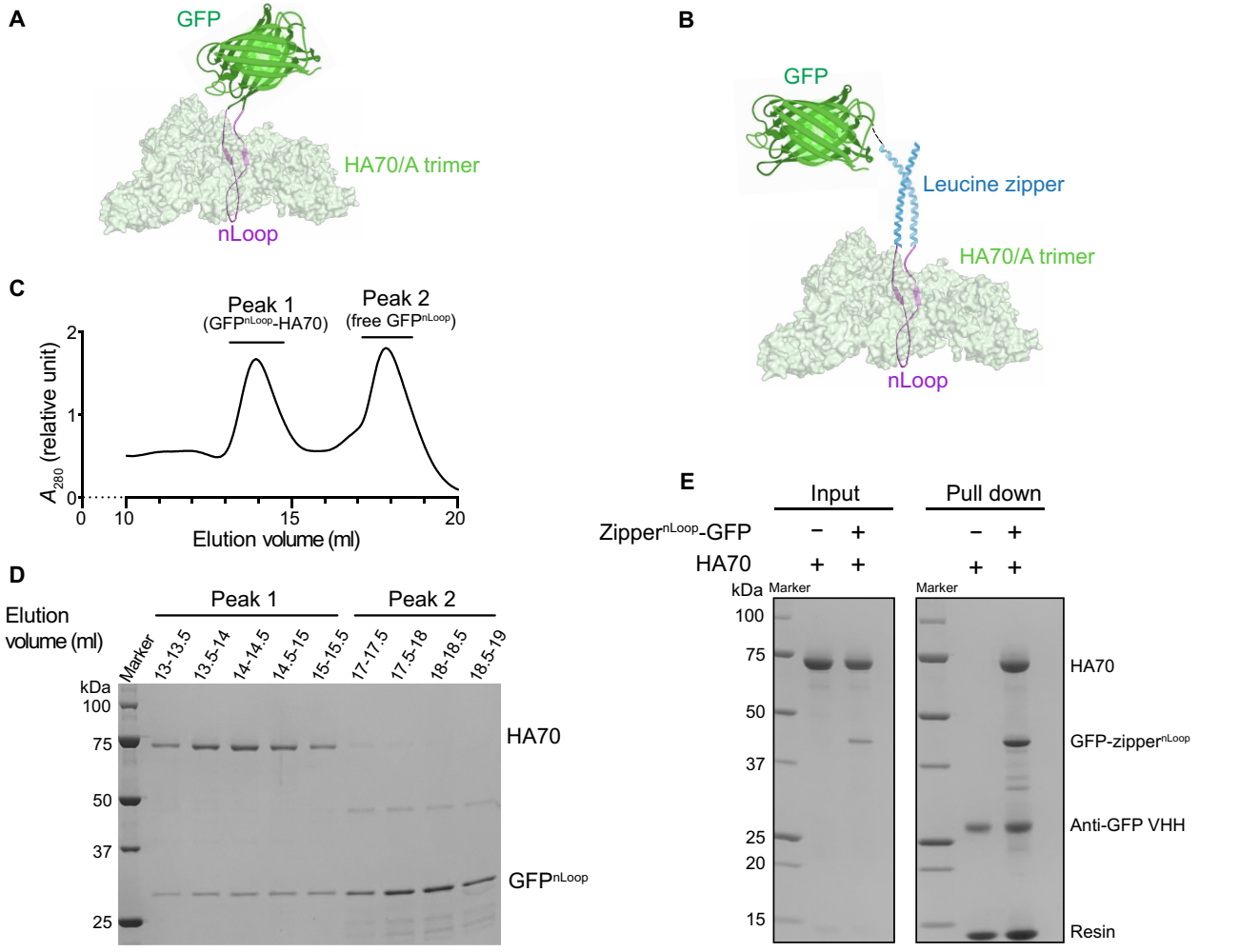

Fig. 8. nLoop is a versatile targeting module that can attach a POI to the HA complex. (**A** and **B**) Schematic illustrations of the engineered GFP^{nLoop} and Zipper^{nLoop}-GFP in complex with HA70/A trimer. Parts of the figure were created using BioRender (Created in BioRender. Liang, L. (2025) https://BioRender.com/xgv3qk1), and the structures are not drawn in proportion. (**C** and **D**) GFP^{nLoop} and HA70/A were coexpressed and copurified, first via the GST-tag on GFP^{nLoop} and then the His-tag on HA70/A. The resulting proteins were analyzed by SEC, and selected fractions from peak 1 (GFP^{nLoop}–HA70/A complex) and peak 2 (free GFP^{nLoop}) were examined by SDS-PAGE. (**E**) Pull-down assay examining the interaction between Zipper^{nLoop}-GFP and HA70/A. His-tagged Zipper^{nLoop}-GFP and His-tagged HA70/A, coexpressed and copurified using Ni-NTA resins, were pulled down using an immobilized anti-GFP VHH as bait and further analyzed by SDS-PAGE.

membrane-spanning β-barrel pore (*49*). We found that the D1 and D2 domain of HA70 share a similar structural fold with monomeric aerolysin and CPE (fig. S8C) (*36*–*38*, *48*). A signature feature of aerolysin is its stem-loop and the two adjacent β-strands, which can undergo a conformational transition to form the transmembrane β-barrel during pore formation (*36*, *48*, *49*). However, HA70 seems to have lost the pore-forming capability as the alternative hydrophobic and hydrophilic residue pattern that is required for interacting with lipid and solvent as observed in aerolysin-like β-pore-forming toxins is not observed in HA70 (fig. S8D). On the other hand, the top layer of the HA70 pseudo-pore contains many hydrophobic residues adapted for binding with the nLoop of NTNH, whereas the corresponding region in aerolysin or CPE is enriched with solvent-exposed charged or polar residues that aid in releasing cellular content following transmembrane pore formation (fig. S8E). Therefore, the pores in HA70 and aerolysin-like toxins have evolved into different functions. Nevertheless, as the double β-barrel channel of aerolysin is believed to provide extra stability for it to resist denaturing conditions (*48*), we suspect that a similar double β-barrel channel of HA70 likely serves to protect both itself and its connection with NTNH from the acidic and protease-rich environment of the GI tract.

Another interesting finding of this study is that the mechanism by which BoNTs exploit the L-PTC to bind host receptors and breach intestinal epithelium resembles that of the AB5 toxins. These are a family of virulence factors for many bacterial pathogens, such as cholera toxin (PDB: 1XTC), *E. coli* heat-labile enterotoxin (PDB: 1LTT), and shiga toxin (PDB: 1DM0) (*50*–*52*). They share a common structural feature in which a monomeric toxin moiety with catalytic activity (A subunit) is tethered to a multimeric B subunit that is responsible for recognizing host receptor on the target cell surface and opening a pathway for the catalytic A subunit to enter host cells (*53*). In this context, the M-PTC mimics the A subunit, while the HA complex is functionally equivalent to the B subunit.

Many AB5 toxins use their B subunits to recognize carbohydrates receptors, reminiscent of the HA complex (*53*–*55*). However, the organization of the L-PTC is unique in a way that its B subunit forms a β-barrel where a β-hairpin of the A subunit is buried, while all AB5 toxins are assembled via a helix or a loop of A subunit that inserts into the α-helical pore of the multimeric B subunits (fig. S9). Moreover, the anchor for attaching to the B subunit is located in the middle of NTNH (nLoop) in the L-PTC, whereas it is found in the terminal regions of the A subunit in AB5 toxins.

We demonstrate that the nLoop can serve as a versatile targeting module to attach a POI to the HA complex, suggesting that we could potentially repurpose BoNT's delivery vehicle for drug delivery applications. As nLoop-containing cargos are "permanently" attached to the HA complex, we believe that this approach would be ideal to deliver therapeutic agents that carry out their activity in the GI lumen, where they are attached to the intestinal epithelium via multivalent carbohydrate binding mediated by the HA complex. We could also use the E-cadherin–binding deficient HA mutants that retain carbohydrate binding ability, so the HA-tethered cargos do not penetrate the intestinal epithelium (*21*). Alternatively, a cargo could be conjugated to the nLoop through a degradable linker, allowing its controlled release into the general circulation following HA-mediated delivery.

In summary, this study reveals a unique nut-and-bolt attachment between NTNH and HA70—a BoNT-like pseudo-toxin and an aerolysin-like pseudo-toxin—that assembles the protective and delivery components into a complete L-PTC. It sets the stage for deeper exploration of BoNT pathogenesis and countermeasure while also paving the way for repurposing the BoNT oral delivery vehicle for targeted drug delivery.

MATERIALS AND METHODS

Cloning, protein expression, and purification

The genes corresponding to BoNT/Ai (E224Q/R363A/Y366F) and NTNH/A1 were cloned into pGEX-6p-1 expression vector with an N-terminal GST-tag followed by a 3C cleavage site. For the mutagenesis studies, the genes of NTNH/A variants were cloned into pCGFP vector with an N-terminal GFP, followed by a thrombin cleavage site. The genes of HA70/A and its variants were cloned into pCDFduet vector with a C-terminal His-tag. The genes encoding NTNH/A1 (strain 62A, prot ID CAA63550), NTNH/A2 (strain Friedrichshain, identical to prot ID ACO85717 of strain Kyoto-F), NTNH/B1 (strain Okra, prot ID ACA47084), NTNH/D (strain 1873, prot ID BAA75083), and NTNH/G (strain CECT4615, prot ID CAA61228) and the genes encoding the respective HA70s were either synthesized with codon usage optimized for *E. coli* expression (Geneart, Regensburg, Germany) and/or amplified by polymerase chain reaction using the genomic DNA of *C. botulinum* strains. NTNH encoding genes were cloned into the pQE (QIAGEN) expression vector with an N-terminal 6×His-tag fused to a thrombin cleavage site and a C-terminal Strep-tag yielding pH6tNTNHA-AS, pH6tNTNHA-A2S, pH6tNTNHA-BS, pH6tNTNHA-DS, and pH6tNTNHA-GS. pH6tNTNHA-AS$^{\Delta nLoop}$ and pH6tNTNH-A2S^{nLoop} were generated by the Genetailor method. The genes encoding the corresponding HA70/A, HA70/B, HA70/D, and HA70/G were cloned into the pRSFDuet-1 dual expression vector (Novagen) with an N-terminal 6×His-tag and a thrombin cleavage site.

BoNT/Ai, NTNH/A variants, and HA70/A variants were expressed in the BL21 Star (DE3) strain of *E. coli* (Invitrogen). In particular, NTNH/A and HA70/A were cotransformed into bacteria and coexpressed. Bacteria were initially cultured at 37°C in LB medium. When an optical density at 600 nm (OD_{600}) reached 0.4 to 0.6, the temperature was decreased to 18°C, and protein expression was induced with 1 mM isopropyl-β-D-thiogalactopyranoside (IPTG). The cells were harvested 16 hours postinduction by centrifugation and stored at −20°C until use. The catalytically inactivated BoNT/Ai was first purified using Glutathione Sepharose 4B resins (GE Healthcare), followed by the removal of the GST-tag through 3C protease on-column cleavage in a buffer containing 50 mM tris (pH 8.0) and 400 mM NaCl. For purification of the NTNH–HA70 complex, proteins were first bound to a Ni-NTA (QIAGEN) affinity column in a buffer containing 50 mM tris (pH 8.0) and 400 mM NaCl and subsequently eluted in the same buffer containing 300 mM imidazole. The eluted fractions were then incubated with Glutathione Sepharose 4B resins (GE Healthcare), followed by on-column cleavage for GST-tag removal. All proteins were further purified through SEC on a Superdex 200 column (GE Healthcare) in a buffer composed of 50 mM MES (pH 6.0) and 200 mM NaCl. To assemble the M-PTC–HA70 complex, the purified NTNH–HA70 complex was mixed with the purified BoNT/Ai in 1:1 molar ratio and further purified by SEC in a buffer containing 50 mM MES (pH 6.0) and 200 mM NaCl. The peak fractions of the complex were concentrated and stored at −80°C for future use.

Crystallization, data collection, and processing

Two anti-BoNT/A VHHs (VHH-F12 and VHH-H7) and one anti-NTNH/A Fab were used to facilitate crystallization. The two VHHs were prepared as previously described (*43*), and the Fab was obtained from B.G.D.'s laboratory (Robert Koch Institute, Germany). The purified M-PTC–HA70 complex (~5 mg/ml) was mixed with VHH-F12, VHH-H7, and the Fab in a molar ratio of 1:1.5:1.5:1.2 for crystallization. Initial crystallization screens were performed using a Gryphon crystallization robot (Art Robbins Instruments) and high-throughput crystallization screen kits (Hampton Research, QIAGEN, or Emerald BioSystems), followed by extensive manual optimization. The best single crystals were grown at 18°C by the hanging drop vapor diffusion method in 1:1 (v/v) ratio with a reservoir solution containing 1.1 M ammonium sulfate and 0.1 M Na acetate (pH 5). The crystals were cryoprotected in their original mother liquor supplemented with 20% (v/v) glycerol and flash-frozen in liquid nitrogen for data collection.

The x-ray diffraction dataset was collected at 100 K at the NE-CAT beamline 24-ID-E, Advanced Photon Source (APS), Argonne National Laboratory using detector ADSC Q315. The data were processed with XDS as implemented in RAPD (https://github.com/RAPD/RAPD) (*56*). The complex structure was solved by the molecular replacement software PHENIX.Phaser-MR (*57*) using the structures of M-PTC/A–VHH-F12 (PDB: 3V0A) (*4*), VHH-H7 (PDB: 6UL6) (*40*), Fab (PDB: 2Z4Q) (*58*), and HA70/A (PDB: 4LO4) (*7*) as the search models. Further refinements of the structures were performed by PHENIX.refine (*59*) and COOT (*60*) in an iterative manner. All the refinement progress was monitored with the free *R* value using a 5% randomly selected test set (*61*). The structures were validated by MolProbity (*62*). The statistics of data collection and structural refinement are summarized in table S1. All structure figures were prepared by PyMOL (www.pymol.org).

Sequence alignment was made using Clustal Omega (*63*) and ESPript 3 (*64*).

Coexpression of NTNH and HA70 and pull-down studies

WT His-GFP-NTNH/A and HA70/A-His or the various combinations of mutants were cotransformed and coexpressed in *E. coli* BL21-Star. The proteins were purified by Ni-NTA resins using binding and wash buffers containing 400 mM NaCl, 50 mM tris (pH 8.0), 5 mM imidazole, and 0.4 mM phenylmethylsulfonyl fluoride (PMSF) and eluted in a buffer containing 400 mM NaCl, 50 mM tris (pH 8.0), and 150 mM imidazole. The SDS-PAGE analysis of the partially purified proteins indicated that HA70/A was expressed at a higher level compared to NTNH/A in all cases. An anti-NTNH/A monoclonal antibody, the same one used for crystallization, was immobilized on CNBr resins to capture NTNH/A in pull-down assays. To test the potential complex formation between variants of NTNH/A and HA70/A, the partially purified proteins were incubated with immobilized NTNH/A in PBST (PBS + 0.01% Tween 20) buffer for 30 min at room temperature. The resins were then washed extensively with PBST buffer for three times, and the bound proteins were denatured by SDS loading buffer and analyzed by SDS-PAGE. The intensities of protein bands were quantified by ImageJ, and the intensity ratio of HA70/A-His:His-GFP-NTNH/A was calculated for comparison. The experiments were performed in triplicates.

For coexpression of NTNH and HA70 across different BoNT serotypes, cultures of *E. coli* BL21 (DE3) transformed with pH6tNTNHA-xS plasmids were additionally transformed with pRSF-H6tHA70-x plasmids and grown in 600 ml of 2YT medium [tryptone (16 g/liter), yeast extract (10 g/liter), and NaCl (5 g/liter)] with ampicillin and kanamycin at 37°C until the OD_{600} of the culture reached 0.6 to 0.8. After induction with 1 mM IPTG (Roth), cultures were incubated overnight at 22°C until harvest. Cell pellets were resuspended in 23 ml of 0.1 M tris-HCl (pH 8.0), containing the protease inhibitors pepstatin A (1 mM), benzamidine (5 mM), and PMSF (0.5 mM) and lysed by ultrasonic treatment for 7 min using 0.5 cycles with 100% amplitude (Hielscher UP200S). The clear lysate was first applied to Co^{2+}-Talon matrix (Takara Bio Europe S.A.S., France) and the eluate subsequently to StrepTactin-Sepharose resin (IBA GmbH, Germany) following the manufacturers' instructions. Fractions were analyzed via SDS-PAGE and Coomassie staining.

Protein engineering by inserting the nLoop to POIs

The gene encoding NTNH/A1 nLoop (Y112–A148) was cloned into NTNH/E between residues E111 and D116 in pGEX-6p-1 vector (termed NTNH/E^{nLoop}), with an N-terminal GST-tag followed by a 3C cleavage site. Residues G116 to G149 of the NTNH/A1 nLoop were inserted into NTNH/A2 between residues G115 and D116 based on pH6tNTNHA-A2S (termed NTNH/$A2^{nLoop}$). The GST-tagged NTNH/E^{nLoop} was co-expressed with the His-tagged HA70/A. The expressed proteins were first purified by Ni-NTA resins and the eluted fraction was further purified by GST resins, followed by on-column 3C protease cleavage for GST-tag removal. The His/Strep-tagged NTNH/$A2^{nLoop}$ was coexpressed with the His-tagged HA70/A. The cleared lysate was applied first to Co^{2+}-Talon matrix (Takara Bio Europe S.A.S., France) and the eluate subsequently to StrepTactin-Sepharose resin (IBA GmbH, Germany). Fractions were analyzed via SDS-PAGE and Coomassie staining.

The purified NTNH/E^{nLoop}–HA70/A complex was further mixed with BoNT/Ei in a 1:1 molar ratio in a buffer containing 50 mM MES (pH 6) and 100 mM NaCl to assemble the M-PTC/E^{nLoop}–HA70/A complex. Negative staining EM study of the M-PTC/E^{nLoop}–HA70/A complex was performed at UC Irvine Materials Research Institute (UC IMRI). The protein samples were prepared for EM using the conventional negative staining method and were imaged at room temperature using a JEOL JEM-2100F TEM and operated at an acceleration voltage of 200 kV. Images were taken under low-dose conditions at a magnification of ×50,000 with a defocus value of −2 μm using a Gatan 4K × 4K charge-coupled device camera, yielding final micrographs with 1.7 Å/pixel. The collected micrographs were imported into CryoSPARC for image processing including: Contrast Transfer Function estimation, particle picking, 2D classification, and ab initio 3D reconstruction (*65*). The 3D reconstruction map of the M-PTC/E^{nLoop}–HA70/A complex was visualized using UCSF ChimeraX (*66*). The "fit-in-map" option in ChimeraX was used to dock the crystal structures of M-PTC/E (PDB: 4ZKT) and HA70/A [PDB: 4LO4 (*7*)] into the 3D density map.

For the GFP^{nLoop} construct, the nLoop (Y112–A148) was inserted between V171 and G174 of Superfolder GFP and together were cloned into a pGEX-6p-1 vector, with an N-terminal GST-tag followed by a 3C cleavage site. The coexpressed GST-tagged GFP^{nLoop} and the His-tagged HA70/A were first purified using glutathione resins, followed by on-column cleavage of the GST-tag on GFP^{nLoop}. The resulting proteins were further purified using Ni-NTA resins. The complex was examined by SEC, and the purity of selected fractions was examined by SDS-PAGE. For the $Zipper^{nLoop}$-GFP construct, the nLoop (Y112–A148) was inserted in a loop connecting two alpha helices in a leucine zipper. They were cloned together into the pCGFP vector and fused with a C-terminal GFP followed by a His-tag. The His-tagged $zipper^{nLoop}$-GFP and the His-tagged HA70/A were coexpressed and purified by Ni-NTA resins. The complexes were examined by pull-down assays using immobilized anti-GFP VHH as bait. The stand-alone HA70/A was used as a negative control. The results were manifested by SDS-PAGE.

Supplementary Materials

The PDF file includes:

Figs. S1 to S9

Table S1

Other Supplementary Material for this manuscript includes the following:

Source data

REFERENCES AND NOTES

1. O. Rossetto, M. Pirazzini, C. Montecucco, Botulinum neurotoxins: Genetic, structural and mechanistic insights. *Nat. Rev. Microbiol.* **12**, 535–549 (2014).
2. M. W. Peck, T. J. Smith, F. Anniballi, J. W. Austin, L. Bano, M. Bradshaw, P. Cuervo, L. W. Cheng, Y. Derman, B. G. Dorner, A. Fisher, K. K. Hill, S. R. Kalb, H. Korkeala, M. Lindstrom, F. Lista, C. Luquez, C. Mazuet, M. Pirazzini, M. R. Popoff, O. Rossetto, A. Rummel, D. Sesardic, B. R. Singh, S. C. Stringer, Historical perspectives and guidelines for botulinum neurotoxin subtype nomenclature. *Toxins* **9**, 38 (2017).
3. K. K. Hill, G. Xie, B. T. Foley, T. J. Smith, A. C. Munk, D. Bruce, L. A. Smith, T. S. Brettin, J. C. Detter, Recombination and insertion events involving the botulinum neurotoxin complex genes in *Clostridium botulinum* types A, B, E and F and *Clostridium butyricum* type E strains. *BMC Biol.* **7**, 66 (2009).
4. S. Gu, S. Rumpel, J. Zhou, J. Strotmeier, H. Bigalke, K. Perry, C. B. Shoemaker, A. Rummel, R. Jin, Botulinum neurotoxin is shielded by NTNHA in an interlocked complex. *Science* **335**, 977–981 (2012).

5. K. H. Lam, R. Jin, Architecture of the botulinum neurotoxin complex: A molecular machine for protection and delivery. *Curr. Opin. Struct. Biol.* **31**, 89–95 (2015).
6. S. Gu, R. Jin, Assembly and function of the botulinum neurotoxin progenitor complex. *Curr. Top Microbiol. Immunol.* **364**, 21–44 (2013).
7. K. Lee, S. Gu, L. Jin, T. T. Le, L. W. Cheng, J. Strotmeier, A. M. Kruel, G. Yao, K. Perry, A. Rummel, R. Jin, Structure of a bimodular botulinum neurotoxin complex provides insights into its oral toxicity. *PLOS Pathog.* **9**, e1003690 (2013).
8. L. Gao, M. B. Nowakowska, K. Selby, A. Przykopanski, B. Chen, M. Kruger, F. P. Douillard, K. H. Lam, P. Chen, T. Huang, N. P. Minton, M. B. Dorner, B. G. Dorner, A. Rummel, M. Lindstrom, R. Jin, Botulinum neurotoxins exploit host digestive proteases to boost their oral toxicity via activating OrfXs/P47. *Nat. Struct. Mol. Biol.* **32**, 864–875 (2025).
9. S. Eswaramoorthy, J. Sun, H. Li, B. R. Singh, S. Swaminathan, Molecular assembly of *clostridium botulinum* progenitor M complex of type E. *Sci. Rep.* **5**, 17795 (2015).
10. M. Martinez-Carranza, J. Skerlova, P. G. Lee, J. Zhang, A. Krc, A. Sirohiwal, D. Burgin, M. Elliott, J. Philippe, S. Donald, F. Hornby, L. Henriksson, G. Masuyer, V. R. I. Kaila, M. Beard, M. Dong, P. Stenmark, Activity of botulinum neurotoxin X and its structure when shielded by a non-toxic non-hemagglutinin protein. *Commun. Chem.* **7**, 179 (2024).
11. S. Kosenina, J. Skerlova, S. Zhang, M. Dong, P. Stenmark, The cryo-EM structure of the BoNT/Wo-NTNH complex reveals two immunoglobulin-like domains. *FEBS J.* **291**, 676–689 (2023).
12. D. A. Benefield, S. K. Dessain, N. Shine, M. D. Ohi, D. B. Lacy, Molecular assembly of botulinum neurotoxin progenitor complexes. *Proc. Natl. Acad. Sci. U.S.A.* **110**, 5630–5635 (2013).
13. I. Ohishi, S. Sugii, G. Sakaguchi, Oral toxicities of *Clostridium botulinum* toxins in response to molecular size. *Infect. Immun.* **16**, 107–109 (1977).
14. L. W. Cheng, B. Onisko, E. A. Johnson, J. R. Reader, S. M. Griffey, A. E. Larson, W. H. Tepp, L. H. Stanker, D. L. Brandon, J. M. Carter, Effects of purification on the bioavailability of botulinum neurotoxin type A. *Toxicology* **249**, 123–129 (2008).
15. Y. Sakaguchi, K. Inoue, T. Ohyama, T. Watanabe, H. Arimitsu, N. Mahmut, K. Oguma, Y. Fujinaga, K. Inoue, K. Honke, *Clostridium botulinum* type A haemagglutinin-positive progenitor toxin (HA+-PTX) binds to oligosaccharides containing Galβ1-4GlcNAc through one subcomponent of haemagglutinin (HA1). *Microbiology* **147**, 811–819 (2001).
16. Y. Fujinaga, K. Inoue, S. Watanabe, K. Yokota, Y. Hirai, E. Nagamachi, K. Oguma, The haemagglutinin of *Clostridium botulinum* type C progenitor toxin plays an essential role in binding of toxin to the epithelial cells of guinea pig small intestine, leading to the efficient absorption of the toxin. *Microbiology* **143** (Pt 12), 3841–3847 (1997).
17. Y. Fujinaga, K. Inoue, S. Watarai, Y. Sakaguchi, H. Arimitsu, J. C. Lee, Y. Jin, T. Matsumura, Y. Kabumoto, T. Watanabe, T. Ohyama, A. Nishikawa, K. Oguma, Molecular characterization of binding subcomponents of *Clostridium botulinum* type C progenitor toxin for intestinal epithelial cells and erythrocytes. *Microbiology* **150**, 1529–1538 (2004).
18. S. Kojima, H. Eguchi, T. Ookawara, N. Fujiwara, J. Yasuda, K. Nakagawa, T. Yamamura, K. Suzuki, *Clostridium botulinum* type A progenitor toxin binds to Intestine-407 cells via N-acetyllactosamine moiety. *Biochem. Biophys. Res. Commun.* **331**, 571–576 (2005).
19. K. Lee, K. H. Lam, A. M. Kruel, K. Perry, A. Rummel, R. Jin, High-resolution crystal structure of HA33 of botulinum neurotoxin type B progenitor toxin complex. *Biochem. Biophys. Res. Commun.* **446**, 568–573 (2014).
20. T. Nakamura, N. Takada, T. Tonozuka, Y. Sakano, K. Oguma, A. Nishikawa, Binding properties of *Clostridium botulinum* type C progenitor toxin to mucins. *Biochim. Biophys. Acta* **1770**, 551–555 (2007).
21. K. Lee, X. Zhong, S. Gu, A. M. Kruel, M. B. Dorner, K. Perry, A. Rummel, M. Dong, R. Jin, Molecular basis for disruption of E-cadherin adhesion by botulinum neurotoxin A complex. *Science* **344**, 1405–1410 (2014).
22. T. Matsumura, Y. Jin, Y. Kabumoto, Y. Takegahara, K. Oguma, W. I. Lencer, Y. Fujinaga, The HA proteins of botulinum toxin disrupt intestinal epithelial intercellular junctions to increase toxin absorption. *Cell Microbiol.* **10**, 355–364 (2008).
23. Y. Sugawara, M. Yutani, S. Amatsu, T. Matsumura, Y. Fujinaga, Functional dissection of the *Clostridium botulinum* type B hemagglutinin complex: Identification of the carbohydrate and E-Cadherin binding sites. *PLOS ONE* **9**, e111170 (2014).
24. Y. Sugawara, T. Matsumura, Y. Takegahara, Y. Jin, Y. Tsukasaki, M. Takeichi, Y. Fujinaga, Botulinum hemagglutinin disrupts the intercellular epithelial barrier by directly binding E-cadherin. *J. Cell Biol.* **189**, 691–700 (2010).
25. S. Amatsu, Y. Sugawara, T. Matsumura, K. Kitadokoro, Y. Fujinaga, Crystal structure of *Clostridium botulinum* whole hemagglutinin reveals a huge triskelion-shaped molecular complex. *J. Biol. Chem.* **288**, 35617–35625 (2013).
26. T. Matsumura, Y. Sugawara, M. Yutani, S. Amatsu, H. Yagita, T. Kohda, S. Fukuoka, Y. Nakamura, S. Fukuda, K. Hase, H. Ohno, Y. Fujinaga, Botulinum toxin A complex exploits intestinal M cells to enter the host and exert neurotoxicity. *Nat. Commun.* **6**, 6255 (2015).
27. M. B. Nowakowska, F. P. Douillard, M. Lindstrom, Looking for the X factor in bacterial pathogenesis: Association of *orfX*-p47 gene clusters with toxin genes in clostridial and non-clostridial bacterial species. *Toxins* **12**, 19 (2019).
28. R. Fujita, Y. Fujinaga, K. Inoue, H. Nakajima, H. Kumon, K. Oguma, Molecular characterization of two forms of nontoxic-nonhemagglutinin components of *Clostridium botulinum* type A progenitor toxins. *FEBS Lett.* **376**, 41–44 (1995).
29. T. Ohyama, T. Watanabe, Y. Fujinaga, K. Inoue, H. Sunagawa, N. Fujii, K. Inoue, K. Oguma, Characterization of nontoxic-nonhemagglutinin component of the two types of progenitor toxin (M and L) produced by *Clostridium botulinum* type D CB-16. *Microbiol. Immunol.* **39**, 457–465 (1995).
30. K. Miyata, T. Yoneyama, T. Suzuki, H. Kouguchi, K. Inui, K. Niwa, T. Watanabe, T. Ohyama, Expression and stability of the nontoxic component of the botulinum toxin complex. *Biochem. Biophys. Res. Commun.* **384**, 126–130 (2009).
31. K. H. Eisele, K. Fink, M. Vey, H. V. Taylor, Studies on the dissociation of botulinum neurotoxin type A complexes. *Toxicon* **57**, 555–565 (2011).
32. H. Kouguchi, T. Watanabe, Y. Sagane, H. Sunagawa, T. Ohyama, In vitro reconstitution of the *Clostridium botulinum* type D progenitor toxin. *J. Biol. Chem.* **277**, 2650–2656 (2002).
33. Y. Sagane, T. Watanabe, H. Kouguchi, H. Sunagawa, S. Obata, K. Oguma, T. Ohyama, Spontaneous nicking in the nontoxic-nonhemagglutinin component of the *Clostridium botulinum* toxin complex. *Biochem. Biophys. Res. Commun.* **292**, 434–440 (2002).
34. S. Yamashita, H. Yoshida, N. Uchiyama, Y. Nakakita, S. Nakakita, T. Tonozuka, K. Oguma, A. Nishikawa, S. Kamitori, Carbohydrate recognition mechanism of HA70 from *Clostridium botulinum* deduced from X-ray structures in complexes with sialylated oligosaccharides. *FEBS Lett.* **586**, 2404–2410 (2012).
35. G. Yao, K. Lee, S. Gu, K. H. Lam, R. Jin, Botulinum neurotoxin a complex recognizes host carbohydrates through its hemagglutinin component. *Toxins* **6**, 624–635 (2014).
36. N. Cirauqui, L. A. Abriata, F. G. van der Goot, M. Dal Peraro, Structural, physicochemical and dynamic features conserved within the aerolysin pore-forming toxin family. *Sci. Rep.* **7**, 13932 (2017).
37. K. Kitadokoro, K. Nishimura, S. Kamitani, A. Fukui-Miyazaki, H. Toshima, H. Abe, Y. Kamata, Y. Sugita-Konishi, S. Yamamoto, H. Karatani, Y. Horiguchi, Crystal structure of *Clostridium perfringens* enterotoxin displays features of β-pore-forming toxins. *J. Biol. Chem.* **286**, 19549–19555 (2011).
38. D. C. Briggs, C. E. Naylor, J. G. Smedley III, N. Lukoyanova, S. Robertson, D. S. Moss, B. A. McClane, A. K. Basak, Structure of the food-poisoning *Clostridium perfringens* enterotoxin reveals similarity to the aerolysin-like pore-forming toxins. *J. Mol. Biol.* **413**, 138–149 (2011).
39. K. H. Lam, K. Perry, C. B. Shoemaker, R. Jin, Two VHH antibodies neutralize botulinum neurotoxin E1 by blocking its membrane translocation in host cells. *Toxins* **12**, 616 (2020).
40. K. H. Lam, J. M. Tremblay, E. Vazquez-Cintron, K. Perry, C. Ondeck, R. P. Webb, P. M. McNutt, C. B. Shoemaker, R. Jin, Structural insights into rational design of single-domain antibody-based antitoxins against botulinum neurotoxins. *Cell Rep.* **30**, 2526–2539.e6 (2020).
41. J. M. Tremblay, E. Vazquez-Cintron, K. H. Lam, J. Mukherjee, D. Bedenice, C. A. Ondeck, M. T. Conroy, S. M. L. Bodt, B. M. Winner, R. P. Webb, K. Ichtchenko, R. Jin, P. M. McNutt, C. B. Shoemaker, Camelid VHH antibodies that neutralize botulinum neurotoxin serotype E intoxication or protease function. *Toxins* **12**, 611 (2020).
42. G. Yao, K. H. Lam, J. Weisemann, L. Peng, N. Krez, K. Perry, C. B. Shoemaker, M. Dong, A. Rummel, R. Jin, A camelid single-domain antibody neutralizes botulinum neurotoxin A by blocking host receptor binding. *Sci. Rep.* **7**, 7438 (2017).
43. K. H. Lam, J. M. Tremblay, K. Perry, K. Ichtchenko, C. B. Shoemaker, R. Jin, Probing the structure and function of the protease domain of botulinum neurotoxins using single-domain antibodies. *PLOS Pathog.* **18**, e1010169 (2022).
44. N. Fujii, K. Kimura, N. Yokosawa, T. Yashiki, K. Tsuzuki, K. Oguma, The complete nucleotide sequence of the gene encoding the nontoxic component of *Clostridium botulinum* type E progenitor toxin. *J. Gen. Microbiol.* **139**, 79–86 (1993).
45. A. K. East, M. D. Collins, Conserved structure of genes encoding components of botulinum neurotoxin complex M and the sequence of the gene coding for the nontoxic component in nonproteolytic *Clostridium botulinum* type F. *Curr. Microbiol.* **29**, 69–77 (1994).
46. G. Lin, W. H. Tepp, C. L. Pier, M. J. Jacobson, E. A. Johnson, Expression of the *Clostridium botulinum* A2 neurotoxin gene cluster proteins and characterization of the A2 complex. *Appl. Environ. Microbiol.* **76**, 40–47 (2010).
47. Y. Jin, Y. Takegahara, Y. Sugawara, T. Matsumura, Y. Fujinaga, Disruption of the epithelial barrier by botulinum haemagglutinin (HA) proteins - differences in cell tropism and the mechanism of action between HA proteins of types A or B, and HA proteins of type C. *Microbiology* **155**, 35–45 (2009).
48. I. Iacovache, S. De Carlo, N. Cirauqui, M. Dal Peraro, F. G. van der Goot, B. Zuber, Cryo-EM structure of aerolysin variants reveals a novel protein fold and the pore-formation process. *Nat. Commun.* **7**, 12062 (2016).
49. M. Podobnik, M. Kisovec, G. Anderluh, Molecular mechanism of pore formation by aerolysin-like proteins. *Philos. Trans. R. Soc. Lond. B Biol. Sci.* **372**, 20160209 (2017).
50. R. G. Zhang, D. L. Scott, M. L. Westbrook, S. Nance, B. D. Spangler, G. G. Shipley, E. M. Westbrook, The three-dimensional crystal structure of cholera toxin. *J. Mol. Biol.* **251**, 563–573 (1995).

51. T. K. Sixma, S. E. Pronk, K. H. Kalk, B. A. van Zanten, A. M. Berghuis, W. G. Hol, Lactose binding to heat-labile enterotoxin revealed by X-ray crystallography. *Nature* **355**, 561–564 (1992).
52. M. E. Fraser, M. M. Chernaia, Y. V. Kozlov, M. N. James, Crystal structure of the holotoxin from *Shigella dysenteriae* at 2.5 A resolution. *Nat. Struct. Biol.* **1**, 59–64 (1994).
53. T. Beddoe, A. W. Paton, J. Le Nours, J. Rossjohn, J. C. Paton, Structure, biological functions and applications of the AB5 toxins. *Trends Biochem. Sci.* **35**, 411–418 (2010).
54. J. B. Heim, V. Hodnik, J. E. Heggelund, G. Anderluh, U. Krengel, Crystal structures of cholera toxin in complex with fucosylated receptors point to importance of secondary binding site. *Sci. Rep.* **9**, 12243 (2019).
55. K. Sandvig, B. van Deurs, Transport of protein toxins into cells: Pathways used by ricin, cholera toxin and Shiga toxin. *FEBS Lett.* **529**, 49–53 (2002).
56. W. Kabsch, XDS. *Acta Crystallogr. D Biol. Crystallogr.* **66**, 125–132 (2010).
57. A. J. McCoy, R. W. Grosse-Kunstleve, P. D. Adams, M. D. Winn, L. C. Storoni, R. J. Read, Phaser crystallographic software. *J. Appl. Crystallogr.* **40**, 658–674 (2007).
58. K. Makabe, T. Nakanishi, K. Tsumoto, Y. Tanaka, H. Kondo, M. Umetsu, Y. Sone, R. Asano, I. Kumagai, Thermodynamic consequences of mutations in vernier zone residues of a humanized anti-human epidermal growth factor receptor murine antibody, 528. *J. Biol. Chem.* **283**, 1156–1166 (2008).
59. P. D. Adams, P. V. Afonine, G. Bunkoczi, V. B. Chen, I. W. Davis, N. Echols, J. J. Headd, L. W. Hung, G. J. Kapral, R. W. Grosse-Kunstleve, A. J. McCoy, N. W. Moriarty, R. Oeffner, R. J. Read, D. C. Richardson, J. S. Richardson, T. C. Terwilliger, P. H. Zwart, PHENIX: A comprehensive Python-based system for macromolecular structure solution. *Acta Crystallogr. D Biol. Crystallogr.* **66**, 213–221 (2010).
60. P. Emsley, K. Cowtan, Coot: Model-building tools for molecular graphics. *Acta Crystallogr. D Biol. Crystallogr.* **60**, 2126–2132 (2004).
61. A. T. Brunger, Free R value: A novel statistical quantity for assessing the accuracy of crystal structures. *Nature* **355**, 472–475 (1992).
62. V. B. Chen, W. B. Arendall III, J. J. Headd, D. A. Keedy, R. M. Immormino, G. J. Kapral, L. W. Murray, J. S. Richardson, D. C. Richardson, MolProbity: All-atom structure validation for macromolecular crystallography. *Acta Crystallogr. D Biol. Crystallogr.* **66**, 12–21 (2010).
63. F. Madeira, M. Pearce, A. R. N. Tivey, P. Basutkar, J. Lee, O. Edbali, N. Madhusoodanan, A. Kolesnikov, R. Lopez, Search and sequence analysis tools services from EMBL-EBI in 2022. *Nucleic Acids Res.* **50**, W276–W279 (2022).
64. X. Robert, P. Gouet, Deciphering key features in protein structures with the new ENDscript server. *Nucleic Acids Res.* **42**, W320–W324 (2014).
65. A. Punjani, J. L. Rubinstein, D. J. Fleet, M. A. Brubaker, cryoSPARC: Algorithms for rapid unsupervised cryo-EM structure determination. *Nat. Methods* **14**, 290–296 (2017).
66. E. F. Pettersen, T. D. Goddard, C. C. Huang, E. C. Meng, G. S. Couch, T. I. Croll, J. H. Morris, T. E. Ferrin, U. C. S. F. ChimeraX, Structure visualization for researchers, educators, and developers. *Protein Sci.* **30**, 70–82 (2021).

Acknowledgments

Funding: This work was partly supported by National Institute of Health grants R01AI125704 (to R.J.), R01AI173059 (to R.J.), R01GM151334 (to R.J.), and R01AI158503 (to R.J.); the Swiss Federal Office for Civil Protection BABS #353005630 (to A.R.); and the German Federal Ministry of Research, Technology and Space grants 13N15512 (to A.R.) and 13N9601 (to B.G.D). EM studies were performed at the UC IMRI. NE-CAT at the Advanced Photon Source (APS) is supported by a grant from the National Institute of General Medical Sciences (P30 GM124165), and the Eiger 16 M detector on the 24-ID-E beam line is funded by a NIH-ORIP HEI grant (S10OD021527). Use of the APS, an Office of Science User Facility operated for the US Department of Energy (DOE) Office of Science by Argonne National Laboratory, was supported by the US DOE under contract no. DE-AC02-06CH11357. **Author contributions:** Conceptualization: K.-h.L., A.R., and R.J. Methodology and investigation: K.-h.L., L.G., A.P., B.C., T.H., A.-M. B., and K.P. Key reagents: M.B.D., M.K., and B.G.D. Supervision: A.R. and R.J. Writing—original draft: K.-h.L., L.G., A.R., and R.J. Writing—review and editing: K.-h.L., L.G., B.G.D., A.R., and R.J. **Competing interests:** R.J. is a cofounder, shareholder, and consultant of Claruvis Biotech, a shareholder of MingMed Biotech, and the founder of J&Z Consulting. R.J.'s relationship with these companies has been reviewed and approved by the University of California Irvine in accordance with its conflict of interest policies. All other authors declare that they have no competing interests. **Data and materials availability:** The coordinates and structure factors for the M-PTC–HA70–VHH-F12–VHH-H7–Fab complex has been deposited to the PDB under accession code 9EA9. All data needed to evaluate the conclusions in this paper are present in the paper and/or the Supplementary Materials. The NTNH/A-binding monoclonal antibody can be provided by B.G.D. pending scientific review and a completed material transfer agreement through Robert Koch Institute. Requests for this antibody should be submitted to B.G.D. (DornerB@rki.de).

Submitted 20 March 2025
Accepted 25 July 2025
Published 27 August 2025
10.1126/sciadv.adx5831